Available online at www.sciencedirect.com

SciVerse ScienceDirect

Ceramics International 39 (2013) 2889–2901

CERAMICS INTERNATIONAL

www.elsevier.com/locate/ceramint

The PZT system ($PbTi_xZr_{1-x}O_3$, $0 \le x \le 1.0$): High temperature X-ray diffraction studies. Complete x-T phase diagram of real solid solutions (Part 3)

I.N. Andryushina*, L.A. Reznichenko, L.A. Shilkina, K.P. Andryushin, S.I. Dudkina

Research Institute of Physics, Southern Federal University, Rostov-on-Don, Russia

Received 11 September 2012; accepted 18 September 2012
Available online 28 September 2012

Abstract

Based on high temperature x-ray diffraction studies of the PZT system ($PbTi_xZr_{1-x}O_3$, $0.0 \le x \le 1.0$) the complete x-T phase diagram of solid solutions is built, which exhibits peculiar properties due to the real structure of ceramics:

- irregularity of the phase transition line to the paraelectric state, which is more pronounced in the rhombohedral–tetragonal transition region;
- appearance of intermediate "region of indistinct symmetry" at $0.2 \le x \le 1.0$, which forestalls the transition to the non-polar cubic phase at temperature increase;
- formation of two morphotropic regions: contracting (rhombic–rhombohedral) and expanding (rhombohedral–tetragonal) at temperature increase;
- richness of single-symmetry phase diagram fragments by regions of coexistence of phase states.

The homogeneity regions of the real solid solutions contain phase-boundary lines of a new type evidencing of intraphase transitions prevailing in the rhombohedral phase, which show up in the presence of two and more different cell values (preserving the global crystal lattice symmetry).

Keywords: D. PZT; Phase diagram; High temperature; Homogeneity regions

1. Introduction

In [1] we reported the systematic study of the solid solutions (SS) ceramics of the $PbZr_{1-x}Ti_xO_3$ system in the interval of $0.37 \le x \le 0.57$. We have built the x-T ($300 \le T \le 920$ K) phase diagram containing a region of indistinct symmetry in the vicinity of transition to the non-polar cubic phase. It is shown that the SS from this region are characterized by weak distortions and temperature–temporal instability of the crystal lattice. We distinguished three concentration intervals differing in the cell volume jump ΔV values on the transition line from the rhombohedral (tetragonal) phase to the unclear symmetry. We revealed the appearance of three temperature intervals of reciprocal dielectric permittivity dependences governed by the existence of two Curie points at the boundaries between the cubic phase and ferroelectric ones.

The aim of the present work is to build the complete x-T phase diagram of the ($PbZr_xTi_xO_3$) PZT SS system based on the high-temperature x-ray studies and taking into account the peculiarities of the real structure of ceramics.

The objects under study, their synthesis are described in detail in [2]. High-temperature studies were performed by the powder X-ray diffraction technique using the ADP diffractometer (geometry of Bragg-Brentano) with $Cu\mathrm{K}_\alpha$-radiation.

*Correspondence to: Research Institute of Physics, Southern Federal University, Stachki ave. 194, Rostov-on-Don 344090, Russian Federation. Tel.: +7 86 3243 4066.
E-mail address: futur6@mail.ru (I.N. Andryushina).

0272-8842/$ - see front matter © 2012 Elsevier Ltd and Techna Group S.r.l. All rights reserved.
http://dx.doi.org/10.1016/j.ceramint.2012.09.063

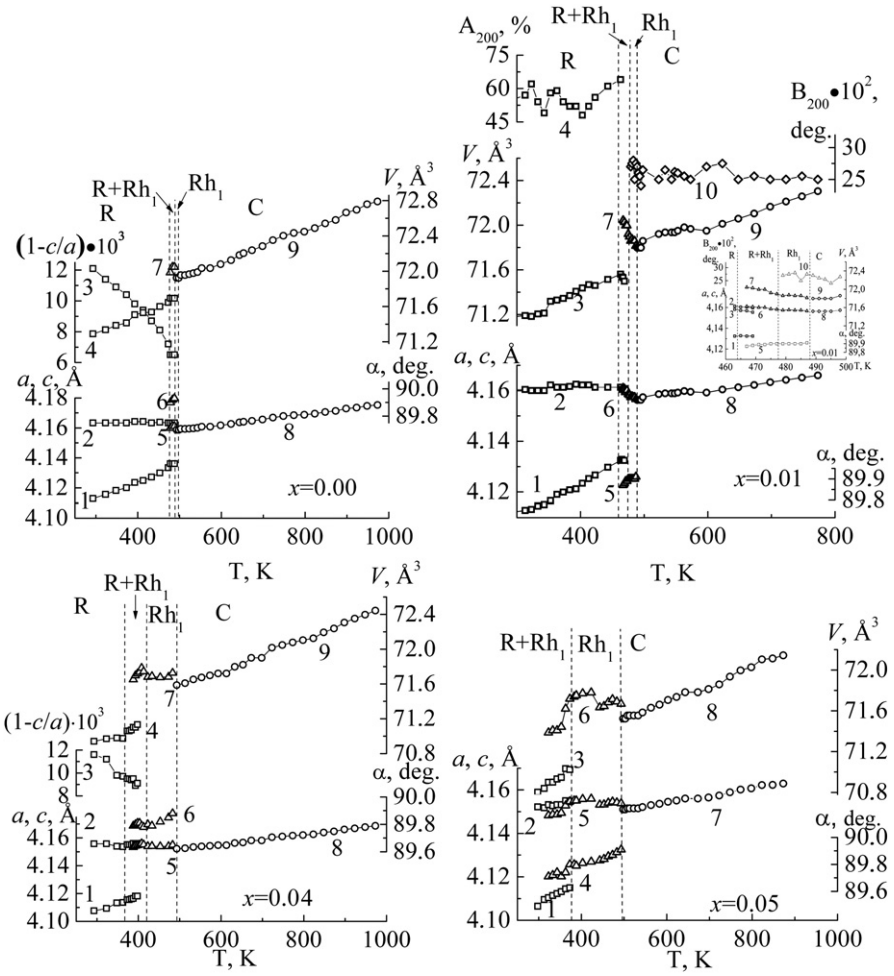

Fig. 1. Temperature dependencies of cell parameters, A-domain fraction degree A_{200}, and half-widths B_{200} of the 200 line for $PbZr_{1-x}Ti_xO_3$ $x=0.00$, 0.01, 0.04, 0.05. SS $x=0.00$, 0.04: pseudotetragonal cell parameters—c (1), a (2), $1-c/a$ (3), V (4), Rh cell parameters—a (5), α (6) and V (7), C cell parameters—a (8), V (9); SS $x=0.01$: pseudotetragonal cell parameters—c (1), a (2), V (3), A_{200} (4), Rh cell parameters—α (5), a (6), C cell parameters—a (8), V (9), B_{200} (10); SS $x=0.05$: pseudotetragonal cell parameters—c (1), a (2), V (3), Rh cell parameters—α (4), a (5), V (6), C cell parameters—a (7), V (8).

2. Experimental results and discussion

2.1. Rhombic region

$PbZrO_3$ Fig. 1($x=0.00$) shows the temperature dependencies of the structural parameters (dotted lines denote regions of indistinct symmetry). To compare the changes in cell volume with temperature at different phases in the rhombic phase parameters pseudotetragonal of perovskite cell were calculated. It can be seen that the rhombic phase (R) preserves up to 488 K, at 478 K the rhombohedral (Rh) phase appears, that is in the range $478 \le T < 488$ K both the phases coexist. Pure Rh phase exists in the range $488 < T < 493$ K, above which the structure becomes cubic (C). The cell volume experiences jumps ΔV at every symmetry change: at $R \rightarrow$ Rh transition $\Delta V = +0.29$ Å^3 and at Rh $\rightarrow C$ transition $\Delta V = -0.12$ Å^3. In the single-phase regions far from the symmetry phase transitions the dependencies $V(T)$ possess monotonic character except for the three temperature intervals, in which the invar effect is observed: one in the R phase 413–433 K and two in the cubic phase—548–573 K and 748–798 K. These evidences of a structural transformation is not accompanied by a symmetry change even in the cubic phase.

$PbZr_{0.99}Ti_{0.01}O_3$. Fig. 1($x=0.01$) shows the temperature dependencies of structural parameters, A-domain fraction degree in the R phase, and 200 x-ray line half-width in the Rh and C phases (dotted lines denote regions of different symmetry). The inset shows the region of $(R+\mathrm{Rh}) \rightarrow C$ transition. The rhombic phase exists in the temperature range 293–477 K, the rhombohedral phase in the range 465–487 K. Thus, these phases coexist in the temperature interval 465–477 K. At $T=489$ K the structure becomes cubic. It should be noted, that the inflection point in the frequency dependencies of $\varepsilon(T)$ in the temperature region preceding the transition to the paraelectric phase coincides with the temperature interval of R and Rh phases coexistence, i.e. corresponds to the antiferroelectric→ferroelectric transition. In contrast to $PbZrO_3$ the dependencies $V(T)$ possess non-monotonic character up to 598 K. In the

intervals 293–343 K, 413–423 K and 533–598 K the cell volume is almost constant, whereas at 353 K it experiences a jump of $+0.12$ Å^3. At the $R \rightarrow$ Rh transition the cell volume increases by 0.51 Å^3, whereas at Rh$\rightarrow C$ one decreases by 0.02 Å^3, which points to the closeness of the latter to the second order phase transition. $A_{200}(T)$ and $B_{200}(T)$ are non-monotonic as well. The decrease of $A_{200}(T)$ in the temperature intervals 323–343 K and 363–403 K is related to the intensity redistribution between the main x-ray reflections 200 and 002 (see Fig. 3a below). The observed changes in the intensity ratio of these reflections are due to the movement of domain boundaries, which results in redistribution of orientational states. Fig. 3 also shows that at $x=0.01$ with the changes in the intensities of the main reflections, the changes in the diffuse character of the wings of x-ray diffraction lines are present (see Fig. 3 a below). At 383 K symmetrical satellites s^- and s^+ appear evidencing the modulation in all $<200>$ directions. At temperature increase the s^- satellite disappears, whereas the s^+ one changes its position with respect to the main reflection 200. Under assumption that the diffuse maximum s^+ is the satellite of the 002 reflection, wavelengths λ of the modulation in this direction was calculated at different temperatures (Table 1).

Appearance of satellites and the change of the modulation wavelength are the characteristic signs of an incommensurate phase, whereas halves of the cells in the modulation wavelength point to the fact that the appearance of incommensurate phase is due to the crystallographic shift planes (CSP) [3]. Similar effects were observed in [4,5] and are, possibly, common to antiferroelectric perovskites. Discontinuous changes of B_{200} in the cubic phase up to 973 K along with constant volume confirms the fact that the cubic phase structure also exhibits changes.

Fig. 1 ($x=0.00$; 0.01; 0.04) shows that at increasing x the existence range of the R phase rapidly shrinks (from 200 K to 80 K), whereas the existence ranges of the mixed and Rh phases widen from 15 K to 50 K and from 5 K to 70 K, respectively.

2.2. Coexistence region of the rhombic and rhombohedral phases of $PbZr_{0.95}Ti_{0.05}O_3$

Fig. 1 ($x=0.05$) shows that, similar to the previous cases, V_{cell} changes with temperature non-monotonically; there are regions of constancy (333–343, 508–533, 643–673 K), sharp increase (353–100 K), and a jump in the single-phase Rh region ($423 < T < 443$ K). The jump value is $\Delta V_{cell} = -0.15$.

After cooling the sample to room temperature from 973 K it does not transform back to the initial state (R + Rh), but becomes single-phase (Rh) (see Fig. 3b below).

Table 1
Modulation wavelengths in the $<200>$ directions and number of cells N_{cell} in one wavelength of $PbTi_{0.01}0Zr_{0.99}O_3$.

T, K	λ, Å	N_{cell}
383	257	62.5
393	257	62.5
403	216	52.5
413	246	59.5
423	266	64.5
443	–	–

2.3. Rhombohedral region

The rhombohedral phase can be split into two regions, which differ strongly by their phase diagrams. The first region is located in the interval $0.10 < x \leq 0.16$ (Fig. 2, a–d) and the second in $0.16 < x \leq 0.36$ (Fig. 2, e–j). In the first region the Rh_1 phase, existing at room temperature, remains up to the transition to the cubic phase, whereas in the second at increasing temperature take place successive changes of single-phase regions and regions of phase states, where phases of the same symmetry coexist [6]. As it can be seen from these figures, the cell volume temperature dependencies change significantly upon x increase. Table 2 gives volume expansion coefficients α of SS from the rhombohedral region in different temperature intervals ΔT.

It is evident from the table that the decrease of α is characteristic for all SS at increasing temperature, as well as increasing Ti concentration except for $x=0.14$. It supports our assumption suggested in [1] that in the PZT system, which contains ions with variable valence (Ti), the influence of component concentration and temperature on the structure of SS is identical, since in both cases the processes occurring in the structure of SS are determined by accumulation, ordering and elimination of oxygen vacancy planes by crystallographic shifts [3].

The decrease of α can be explained by the following. Earlier we have made a suggestion [7] that at $x \geq 0.10$ clusters of a new phase begin to form, in which titanium prevails and which possesses the symmetry different from Rh, presumably tetragonal. Therefore, the increase of temperature, similar to the titanium concentration increase, should result in the increase of the number of tetragonal clusters and, consequently, to the decrease of the average cell size. This effect is pronounced for SS with $x=0.12$, in which α sharply decreases to -2.8×10^{-5} upon approaching the transition temperature to the cubic phase. The change in the vacancy behavior possesses periodic character and therefore α also changes periodically with the increase of the Ti concentration or temperature.

According to [8] the SS with $x=0.35$ is located in the region of the R3c$\rightarrow$R3m phase transition, whereas our data suggest that it belongs to the two-phase region, where two Rh phases coexist. As the x-ray reflection profile analysis reveals (Fig. 3) in this SS two rhombohedral phases are identified due to modulation of interplanar spacings, i.e. due to periodic recurrence of larger d_{max} and smaller d_{min} distances, which results in appearance of

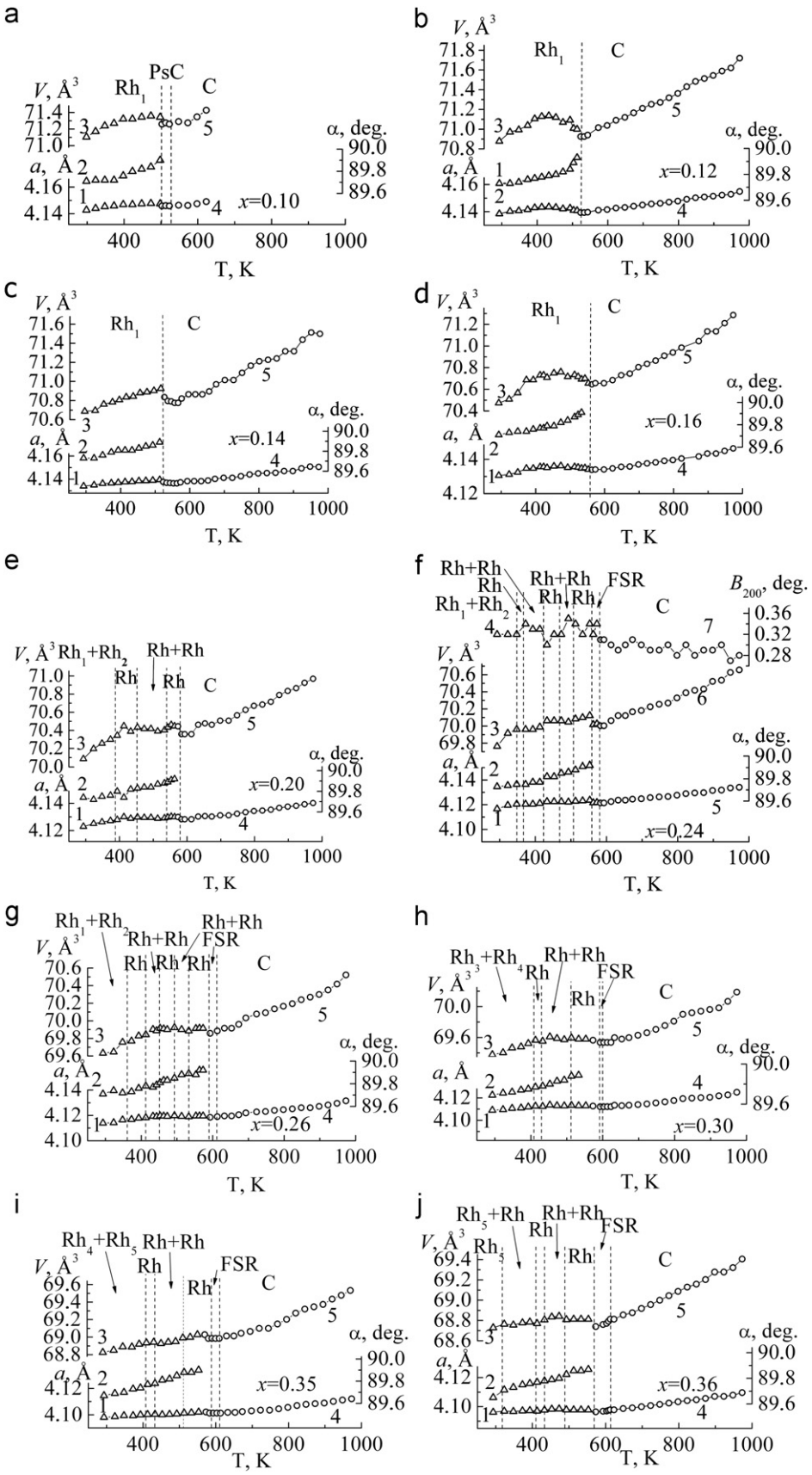

Fig. 2. Temperature dependencies of the cell parameters and cell volume of the $PbTi_xZr_{1-x}O_3$ SS with different component ratios in rhombohedral region: Rh cell parameters—a (1), α (2) and V (3), C cell parameters—a (4), V (5); SS $x=0.24$: Rh cell parameters—a (1), α (2) and V (3), B_{200} (4), C cell parameters—a (5), V (6), B_{200} (7).

Table 2
Temperature coefficients of volume expansion α of SS in the rhombohedral region in different temperature intervals ΔT.

x	ΔT	$\alpha \times 10^5$	ΔT	$\alpha \times 10^5$	ΔT	$\alpha \times 10^5$	ΔT	$\alpha \times 10^5$	ΔT	$\alpha \times 10^5$
0.10	20–75	3.5	75–125	2.4	125–200	0.7				
0.12	20–140	2.9	140–180	−0.3	180–240	−2.8				
0.14	20–50	0.3	50–240	1.7						
0.16	20–140	3.0	140–200	0.7	200–280	−1.8				
0.20	20–140	4.3	140–240	−0.8	240–300	1.3				
0.24	20–75	5.1	75–120	0	120–160	3.5	160–200	0	200–280	1
0.26	20–160	2.8	160–300	0.1						
0.30	20–140	2.3	140–280	0.1						
0.35	20–140	1.5	140–200	0.2	200–280	1.6				
0.36	20–50	1.7	50–140	0.1	140–180	2.4	220–280	−0.3		

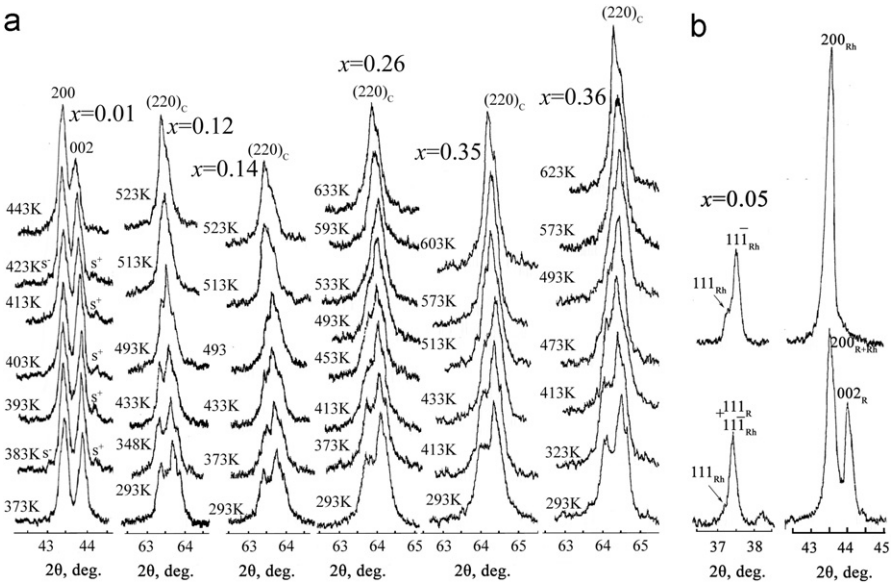

Fig. 3. Diffraction pattern fragments including (a) the $(200)_C$ and $(220)_C$ reflections of SS with (x=0.00–0.36); (b) the $(200)_C$ and $(111)_C$ reflections of SS with (x=0.05) at 298 K: before temperature measuring (bottom); after temperature measuring (top).

additional satellite reflections that are not necessarily symmetrical with respect to the main reflection. It is known that the satellite asymmetry may appear not only due to simultaneous change of the lattice period and structural amplitude [9], but also due to asymmetric profile of the periodic inhomogeneity of interplanar spacings. With the rise of reflection index l the relative intensity of satellites sharply increases and may exceed the intensity of the main reflection [10]. This is seen in Fig. 4, where the profiles of reflections $(222)_c$ and $(220)_c$ of the SS $Pb(Ti_{0.35}Zr_{0.65})O_3$ are shown. The first multiplet consists of the main reflection $22\overline{2}$ and the satellites of the main reflection 222: 222_{max} и 222_{min}. The second multiplet consists of the main reflections 220 and $2\overline{2}0$ and the satellites of the reflection 220: 220_{max} и 220_{min}. At 393 K the parameters of the larger cell are a_{max}=4.102 Å, α=89.63°, V_{max}=69.02 Å^3, of the smaller cell a_{min}=4.097 Å, α=89.84°, V_{min}=68.75 Å^3, and of the middle cell a_{mid}=4.100 Å, α=89.74°, V_{mid}=68.92 Å^3. In the SS with x=0.36 at 373 K, where two Rh phases exist, a satellite of the diffraction line 220 of a higher order is observed (Fig. 4). The modulation wavelengths, calculated according to the s_1 and s_2 satellites position with respect to the main reflection 200, are λ_1=833 Å and λ_2=278 Å and are interrelated by the relation $\lambda_1=3\lambda_2$. Strong satellites of odd order point to domain-like character of the structural modulation of SS.

In [1] we reported the existence of indistinct symmetry region (ISR) in the transition temperature range from the lower symmetry phase to the cubic one, which is characterized by temporally unstable splitting of practically single diffraction line 200 in its maximum without half-width increase. In this study, as can be seen in the phase diagram, ISR appears only for $x > 0.20$. At lower titanium concentrations the transition to the cubic phase occurs directly from the Rh phase.

According to [8] and [11] the tetragonal phase is intermediate for the Rh→C phase transition for SS with $x > 0.20$, which allows the authors to draw a conclusion of the triple point existence close to x=0.22. Our data do not confirm the existence of this tetragonal phase, but the

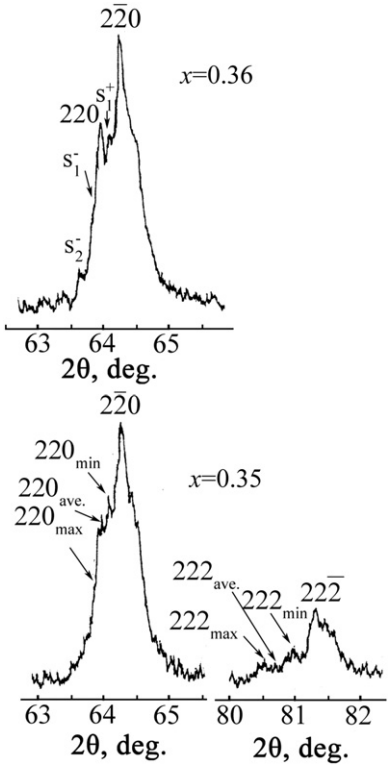

Fig. 4. Diffraction pattern fragments including the $(222)_C$ and $(220)_C$ reflections of SS with ($x=0.35$) at 393 K and $(220)_C$, with ($x=0.36$) at 373 K, illustrating the modulation of structure.

disappearance of ISR exactly at $x\sim0.20$ indicates peculiar character of this point.

The superstructure reflections evidencing of the R3c→R3m transition are not observed by us. Therefore this transition line in the phase diagram is built according to the inflection points of both $V(T)$ and $\alpha(T)$. The diagram shows that in the interval $0.10\le x\le0.20$ the R3c→R3m transition line almost coincides with the data obtained for single crystals [8] except for the SS with $x=0.14$. In the interval $0.20<x<0.36$ due to a big number of transitions from a single-phase state to a two-phase the changes in the cell volume and angle α with temperature possess step-like character. Therefore, the R3c→R3m transition temperature has significant data spread.

Fig. 5 shows the x dependence of the cell volume jump ΔV at the R3m→C phase transition. As mentioned above, the transitions from the R to the Rh phase are accompanied by large cell volume jumps, i.e. are of first order.

The transition to the cubic phase in SS with $x=0.01$ and $x=0.16$ is not accompanied by a jump of V, i.e. is of second order. For $PbZrO_3$ and intervals $0.01<x<0.16$ and $0.16<x<0.30$ the transitions are accompanied by jumps of V, i.e. are of first order. In the concentration interval $0.30\le x\le0.36$ the phase transition is close to the second order.

Thus, as a result of high-temperature studies of SS of the PZT system in the interval $0.0<x<0.36$ the following

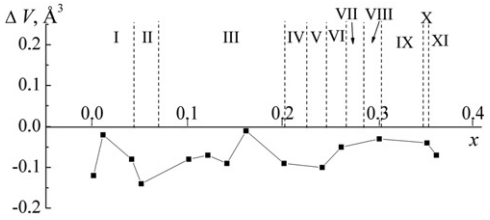

Fig. 5. Dependence of the cell volume jump ΔV on x at R3m→Pm3m phase transition. The phase notation: I—$R(0\le x\le0.04)$; II—$R+Rh_I(0.04<x\le0.065)$; III—$Rh_I(0.065<x\le0.20)$; IV—$Rh_I+Rh_{II}(0.20<x\le0.22)$; V—$Rh_{II}(0.22<x\le0.24)$; VI—$Rh_{II}+Rh_{III}(0.24<x\le0.26)$; VII—$Rh_{III}(0.26<x\le0.28)$; VIII—$Rh_{III}+Rh_{IV}(0.28<x\le0.30)$; IX—$Rh_{IV}(0.30<x\le0.34)$; X—$Rh_{IV}+Rh_V(0.34<x\le0.35)$; XI—$Rh_V(0.35<x\le0.36)$.

fundamental differences from the traditional x-T phase diagram are revealed:

1. For $x>0.2$ the transition to the cubic phase occurs not through the tetragonal phase, but through the region of unclear symmetry, which is characterized by temperature-temporal instability. Upon approaching the MR the width of ISR increases.
2. The rhombohedral phase existing in the interval $0.065\le x\le0.36$ consists of two regions: $0.065\le x\le0.16$ and $0.16\le x\le0.36$. In the first concentration range the Rh_1 phase, existing at room temperature, remains up to the transition to the cubic phase. In the second concentration range successive changes of single-phase regions and regions of coexistence of two phases of the same symmetry, i.e. regions of phase states, take place with temperature increase.

2.4. Tetragonal region

The x-T phase diagram in the tetragonal region of the PZT system, similar to the rhombohedral region, is not uniform: single-phase regions upon increasing temperature give place to regions of phase states coexistence. Fig. 6 shows x-ray fragments including 002 and 200 diffraction lines of SS $x=0.60$, 0.80. It can be seen that the 002 lines, which are single-peaked at room temperature, split into two lines, i.e. a second tetragonal phase appears with a very close c parameter. On the contrary, x-ray lines ($x=0.95$), which are double-peaked at room temperature, become single. Fig. 7(a–j) shows temperature dependencies of cell parameters and volume for SS in the interval $0.60\le x\le1.0$. The peculiarity of these diagrams is that in the tetragonal phase the cell volume does not increase with rising temperature, and what is more, starting with certain own temperature for each SS the cell volume decreases. The two exceptions are SS with $x=0.70$ and 0.75, for which $V(T)$ has no extensive regions of decrease. Let us discuss in detail the structural changes in the SS with $x=0.75$ at increasing temperature. As follows from Fig. 7d, the cell volume does not increase with rising

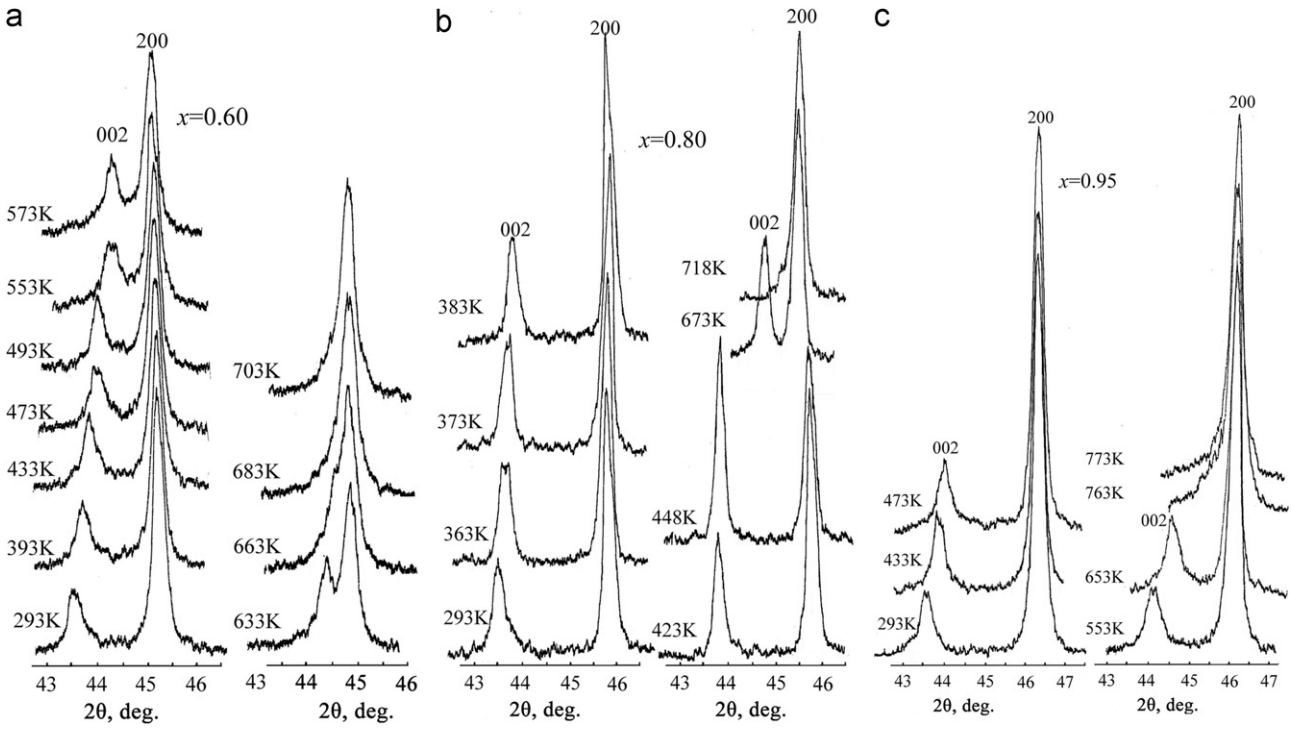

Fig. 6. Diffraction pattern fragments including the 002 and 200 reflections of SS with $x=0.60$, 0.80, 0.95.

temperature as it should, but up to the transition to the cubic phase remains constant exhibiting deviations not exceeding the measurement error. Nevertheless one can distinguish regions of monotonic decrease (433–493)K and (513–553)K, as well as constant volume regions 293–348 K, 493–413 K, and 593–613 K. The latter coincides with temperatures of maxima of $\varepsilon/\varepsilon_o(T)$ at the measuring field frequencies of 0.1–1 kHz. The diffraction patterns corresponding to the regions of changing and constant cell volume are different (Fig. 8a and b). In the former, the isothermal ageing time increase does not lead to any $(200)_c$ line profile changes (Fig. 8, 453 K), whereas in the latter, immediately after reaching the temperature the width of the $(200)_c$ line increased and diffused maxima appeared in the wings of the 002 line, evidencing of the structural modulation in the [001] direction (Fig. 8, 593 K). Upon ageing time increase the 200 line width decreases and the maxima become more diffuse. Similar behavior is observed in other temperature intervals of cell volume constancy. Obviously, the change of the real structure of SS occurs at constant volume. It was shown [12], that the perfection degree and the size of microdomains, as well the type of order in them, change at increasing temperature. As our experiment reveals, these processes take place not continuously, but only at certain temperatures peculiar to the given composition, which allows considering such structural changes as intraphase transformations [13]. Above 723 K the structure of SS with $x=0.75$ becomes cubic, with the cell volume jump $\Delta V=-0.11$ Å^3. In the interval $723\ \mathrm{K} < \mathrm{T} < 973\ \mathrm{K}$ sharp increase of the cell volume is observed and the average volume expansion coefficient is $3.6\times10^{-5}\ \mathrm{K}^{-1}$. However, the inflection points of $V(\mathrm{T})$ at $T=823$ K and 898 K evidence that in the cubic phase the structure also experiences transformations.

On the threshold of a symmetry phase transition, when the tetragonal cell distortion is still distinctly observed in the x-ray diffraction line profiles of solid solutions, the 200 reflection splits into two peaks upon increasing the isothermal ageing time to 10–15 min. One may suppose that the cubic phase appears along with the tetragonal one, however after 20 min of ageing the splitting disappears. Fig. 9 shows this effect for SS with $x=0.70$. It can be seen that at 688 K and 693 K the 200 line splitting is sufficiently large, at 698 K it is significantly smaller, whereas in the interval 703–723 K (after the transition from the tetragonal phase to the cubic one) significant splitting of the 200 reflection is again observed as well as its disappearance upon isothermal ageing time increase. Thus, in the temperature range 688–723 K the structure experiences transient changes of the symmetry or of the phase state of the SS. Moreover, these changes occur in two stages corresponding to forward and backward temperature changes of $T_k(f)$. Similar behavior of the diffraction pattern is typical for all tetragonal SS except for SS with $x=0.80$. Since the crystal lattice changes of SS in this temperature range are characterized by temperature–temporal instability, we refer to this structural state as unclear symmetry region (similar to [13]).

Solid solutions, which exhibit decreasing cell volume V with increasing temperature, are distinguished by the widths of temperature intervals as well as by the rate of decrease of V (Table 3).

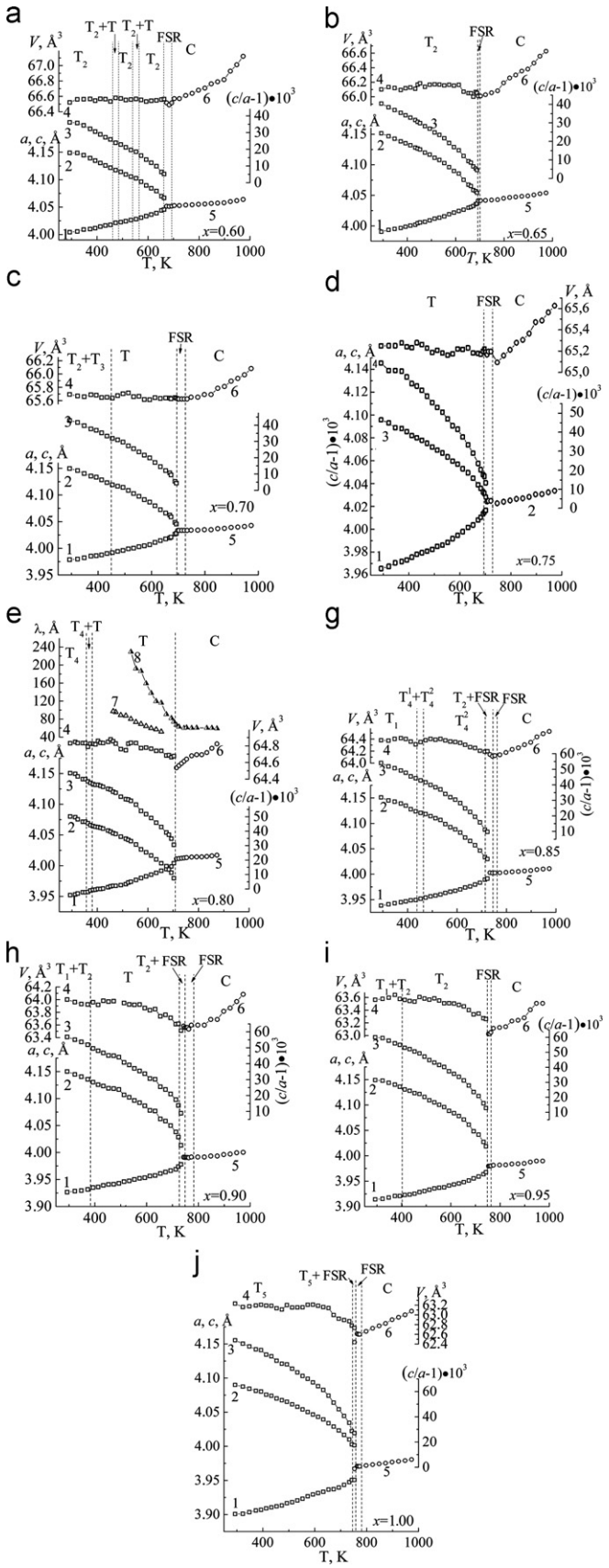

Fig. 7. Temperature dependencies of cell parameters and cell volume for $PbTi_xZr_{1-x}O_3$ SS with $0.60 \le x \le 1.0$: tetragonal cell parameters–a (1), $c/a-1$ (2), c (3), V (4), C cell parameters–a (5), V (6), for SS $x=0.8-\lambda_1$ (7), λ_2 (8) – modulation wavelengths.

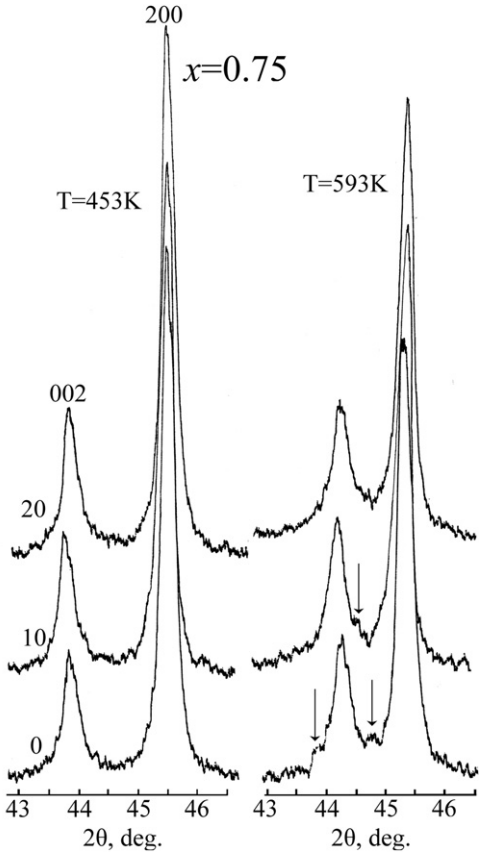

Fig. 8. Diffraction line $(200)_c$ profiles of $PbTi_{0.75}Zr_{0.25}O_3$ SS in the temperature regions of changing (453 K) and constant (593 K) cell volume. The numbers at left on the lines give isothermal ageing times in minutes.

As it is evident from the table, the SS with $x=0.80$ and $x=0.85$ possess the widest temperature ranges and the smallest values of α. This can be explained by the fact that these SS are the least defective, which is in accordance with analogous conclusions drawn from the PZT system study at room temperature.

The temperature dependence $V(T)$ for SS with $x=0.80$ (Fig. 7e) possesses a dip in the interval $463\ \text{K} \le T \le 523\ \text{K}$, which is also characterized by drastic changes in the diffraction pattern. Fig. 10 shows that at 463 K a superstructure line denoted by s_1 appears ahead of the main diffraction line 002. Upon increasing temperature it slowly shifts towards smaller angles θ. Such behavior of a superstructure peak suggests that it is a satellite of the main reflection and its appearance is not related to Zr and Ti ordering in the B-positions. At $T=533$ K a second satellite peak s_2 appears, which, similar to the first one, shifts towards smaller angles θ upon increasing temperature. At $T=593$ K the intensities of both satellites decrease, at 673 K the intensity of s_2 increases, whereas that of s_1 further decreases and at 693 K the s_1 satellite disappears, whereas s_2 persists up to 873 K. Under the assumption that s_1 and s_2 are satellites of the 002 reflection, the modulation wavelengths λ_1 and λ_2 were calculated (Fig. 7e). It can be seen from the figure that in the interval 463–723 K both wavelengths decrease with different rates, whereas after the

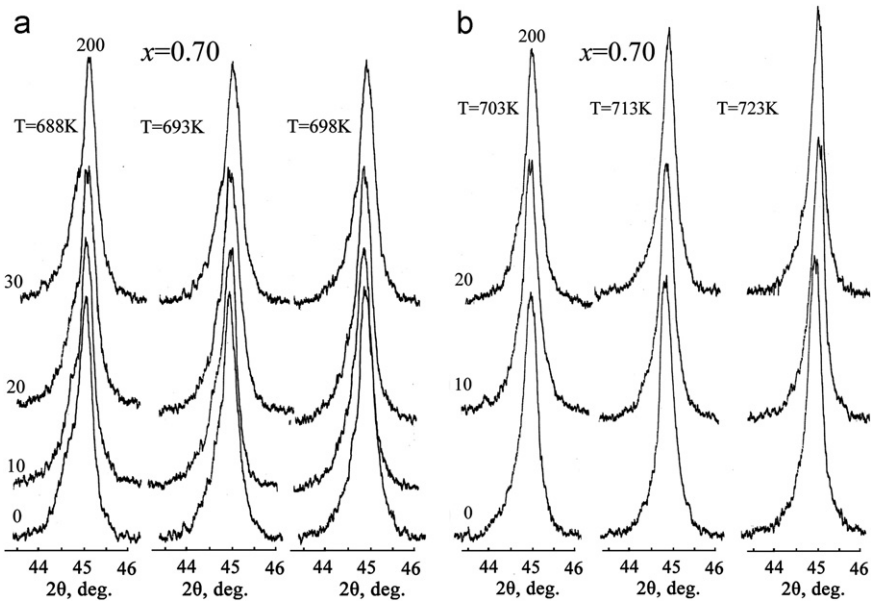

Fig. 9. Changes in the diffraction line $(200)_c$ profile of $PbTi_{0.7}0Zr_{0.30}O_3$ SS depending on the isothermal ageing time in the temperature range $688K \leq T \leq 723K$ (the region of FE→PE transition). The numbers at left on the lines give isothermal ageing times in minutes.

Table 3
Temperature intervals, in which the decrease of V occurs, their widths ΔT, and temperature coefficients of volume expansion α in this region.

x	$\alpha \times 10^5$, K^{-1}	Temperature interval	ΔT
0.60	–	–	–
0.65	−2.5	340–410	70
0.70	–	–	–
0.75	–	–	–
0.80	−1.6	275–430	155
0.85	−2.1	260–420	160
0.90	−4.4	300–450	150
0.95	−3.0	340–470	130
1	−6.5	380–480	100

transition to the cubic phase λ_2 remains constant and equal to ≈ 60 Å, which amounts to 15 cells. It was shown in [14] that in the case of a structural phase transition in a crystal from the state modulated by one displacement wave to a state with another one through intermediate states with different degrees of incommensurability of displacement waves, the positions of satellite peaks should change continuously without appearance of additional intensity peaks. Obviously, an incommensurate phase exists in the SS with $x=0.80$ in the interval $463\,K \leq T \leq 523\,K$, whereas the cell volume decrease unambiguously evidences, that the incommensurate phase appears as a result of crystallographic shift planes (CSP) formation in the structure of SS, since the compaction of ceramics occurs exactly by these planes [15]. Subsequent cell volume increase may be connected with formation of additional point defects, resulting in cell swelling.

The splitting of the 200 diffraction line which is typical for all SS in the temperature range of ISR occurs without

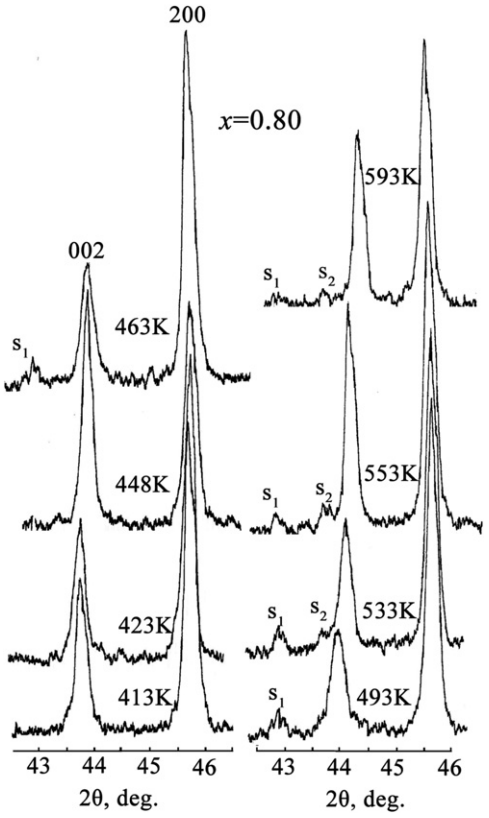

Fig. 10. Diffraction pattern fragments of $PbTi_{0.80}Zr_{0.20}O_3$ SS including the diffraction lines $(200)_c$ and satellites.

half-width increase and has a form of δ-like peaks. δ-like peaks at satellites were observed in other objects studied in [14,16], which was interpreted as matching of initial phases of displacement waves in individual domains by matching

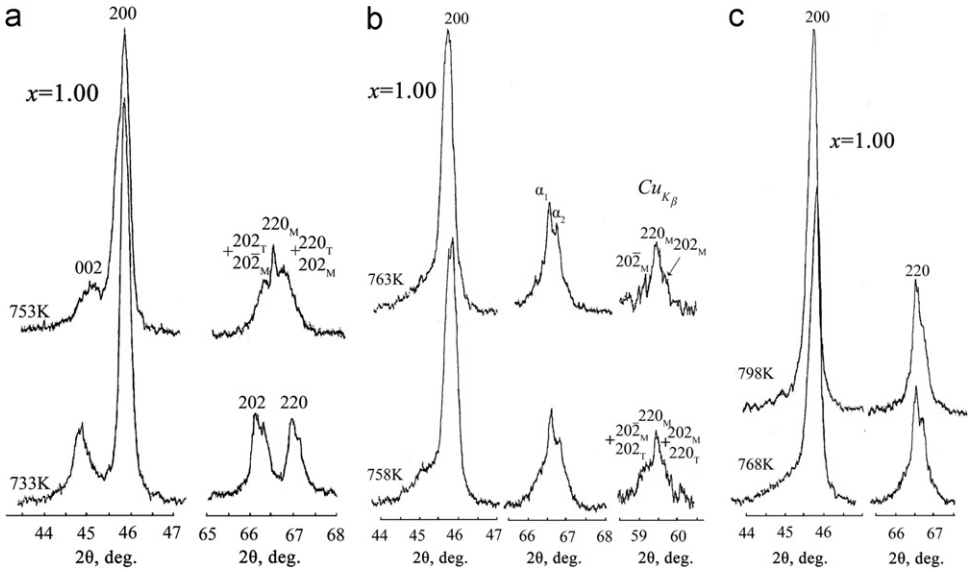

Fig. 11. Diffraction pattern fragments including the $(200)_C$ and $(220)_C$ reflections of $PbTiO_3$ in temperature range 733–798 K. Time of isothermal ageining- 30 min. At 758 K and 763 K presented lines measured at Cu_{K_β} radiation.

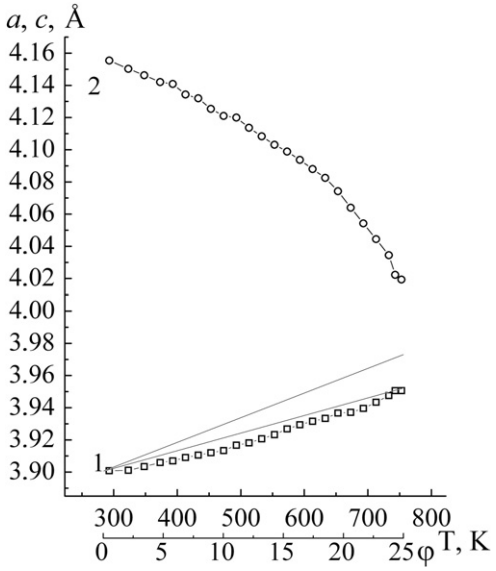

Fig. 12. Temperature dependence of a_{exp} of $PbTiO_3$ (1) and dependence of a_{calc} on the angle φ between the [001] direction and that of Ti^{+4} displacement under the assumption that the displacement of titanium occurs in the {100} planes – upper line, in the {110} planes – lower line; (2) – the c parameter.

density wave of defects. Obviously, in our case the appearance of such peaks is also related to the change of structure modulation character, induced, in turn, by the change of the real structure of solid solutions, namely by rotations of extensive defects (domain boundaries and crystallographic shift planes) and atom displacement directions connected with them [14]. This matter requires a theoretical treatment, but, nevertheless, the results obtained during high-temperature $PbTiO_3$ study confirm the assumption.

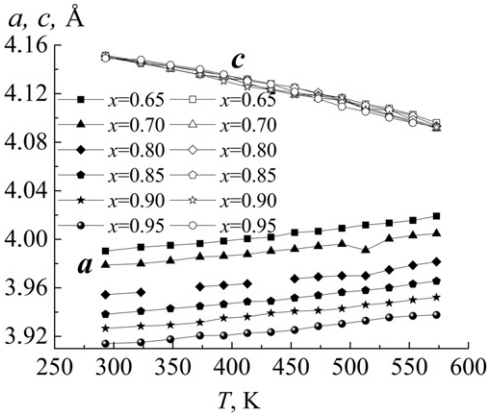

Fig. 13. Temperature dependencies of cell parameters of SS of the PZT system from the tetragonal region.

In [17–19] it was shown, that the tetragonal distortion of the perovskite cell remains above the transition temperature to the paraelectric phase in $PbTiO_3$. In our study the character of the $PbTiO_3$ diffraction pattern change in the vicinity of ferroelectric – paraelectric transition allows the assumption that the transition from the tetragonal phase to the cubic one occurs through a monoclinic phase. The changes in the $(200)_c$ and $(220)_c$ line profiles in the 733–768 K interval are shown in Fig. 11. It can be seen that at 753 K the intensity at maximum sharply decreases and the half-width of the 200 and 002 lines increases (the half-width of 200 at 733 K is 0.26°, at 753 K–0.37°). Between the 202 and 220 lines of the tetragonal phase an additional peak appears, which is usually interpreted as the 220 reflection of the cubic phase. At 758–763 K the T phase, as evident from the $(200)_c$ reflection in the figure, does no longer exist as a well structured form and the

symmetry of SS may be represented as pseudo-cubic. The (220) reflection does not correspond to a pseudo-cubic (very small) cell distortion, which is easily seen in the $(220)_c$ profiles obtained with Cu_{K_β} emission, but to a monoclinic cell distortion with cell parameters $a=\ c=3.973$ Å, $b=3.970$ Å, $\beta=90.45^{\circ}$, $V=62.67$ Å^3 at 763 K. This means that the direction of Ti displacement from the center of the oxygen octahedron along the [001] axis has changed in the T phase and gave a non-zero component along $<100>$, which should result in a parameter increase. It is known, that titanium oxide belongs to a class of infinitely adaptive structures, in which CSP changes its position continuously from one stable position to another through all possible orientations [3]. In [1] we made a suggestion that in perovskite-like structures containing Ti this peculiarity of CSP behavior persists. Thus, when the defective structure changes upon increasing temperature, the change in the Ti displacement direction will occur continuously. We calculated the change in the a parameter under the condition that the Ti displacement direction rotation occurs in the {110} planes. Fig. 12 shows the dependencies of a_{exp} on temperature and a_{calc} on angle φ between the [001] direction and that of the Ti displacement, which changes with increasing temperature. It can be seen that the increases of a_{exp} and a_{calc} coincide well when the change in the Ti displacement direction occurs in the {110} planes. For comparison $a_{calc}(\varphi)$ is given under the condition that the change in the Ti direction occurs in the {100} planes. Therefore, the assumption that the phase transition is the result of the real (defective) structure change seems to us well grounded.

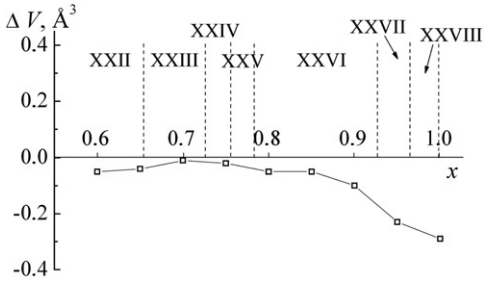

Fig. 14. Dependence of the cell volume jump ΔV on x at $T\rightarrow C$ phase transition. The phase notation at room temperature: XXII—$T_2(0.58 \leq x \leq 0.65)$; XXIII—$T_2+T_3(0.65 < x \leq 0.725)$; XXIV—$T_3(0.725 < x \leq 0.75)$; XXV—$T_3+T_4(0.75 < x \leq 0.775)$; XXVI—$T_4(0.775 \leq x \leq 0.925)$; XXVII—$T_4+T_5(0.925 < x \leq 0.95)$; XXVIII—$T_5(0.95 < x \leq 1)$.

Table 4
The number of invar volume regions and their temperature interval in the cubic phase of SS of the PZT system.

x	Number of invar regions of V	Temperature intervals of the widest invar regions of V, K
0.14	5	593–633; 798–848
0.20	4	573–613; 633–673
0.26	1	723–748
0.30	2	593–623; 633–673
0.35	2	723–748; 633–653
0.36	1	898–923
0.60	1	703–723
0.65	–	
0.70	2	748–773; 798–823
0.75	–	
0.80	1	773–813
0.85	–	
0.90	1	848–873
0.95	2	848–873; 948–973
1.0	–	

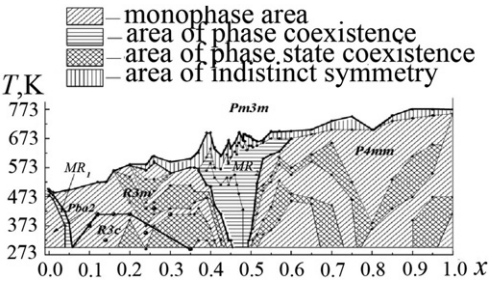

Fig. 15. Complete x-T phase diagram of the real SS of the PZT system.

One of the peculiarities of behavior of structural parameters with increasing temperature is that the cell parameter c at all temperatures does not depend on x. Fig. 13 shows the temperature dependences of cell parameters of SS from the tetragonal region of the PZT system.

It can be seen that in contrast to the parameter a, the parameter c is practically identical for all SS and the maximum (though very subtle) difference is found in the incommensurate phase region. The constancy of the parameter c in the tetragonal region of the PZT system was pointed out earlier [20], where the authors related this fact with stringent dependence of the Zr^{4+} and Ti^{4+} displacements on their average radius.

In opinion of the authors of [20] the decrease of Zr^{4+} and Ti^{4+} displacements upon increasing zirconium concentration is due to the decrease of c/a. The differently directed action of the decreasing displacements of Zr^{4+} and Ti^{4+} and increasing average radius of B cation lead to the constancy of parameter c. However, the authors [20] do not consider the displacement of Pb^{2+}, which amounts to 0.47 Å [21] and is the cause of such a large ratio $c/a=1.063$ in $PbTiO_3$ at room temperature. Our explanations of the c parameter constancy are given in the section devoted to the PZT system study at room temperature and the absence of c dependence on x at high temperatures supports the validity of the assumption.

Fig. 14 shows the cell volume jumps at $T\rightarrow C$ phase transition. It can be seen that up to $x=0.75$ the phase transitions are close to the second kind, whereas at $x=0.70$ $\Delta V=0$, and at $x>0.75$ the phase transitions become first order phase transitions. It should be noted that in [22] in the interval $0.60<x<0.70$ an existence of a tricritical point was established, dividing the regions of first and

second order phase transitions. According to our data this point corresponds to SS with $x=0.70$.

In conclusion one should note that another confirmation of the fact, that the real (defective) structure plays the key role in the changes of the structural and, therefore, electrophysical properties of SS of the PZT system, is that in the paraelectric cubic phase the crystal lattice also experiences changes. This is evidenced by the fact that above T_c the dependencies $V(T)$ possess inflection points and invar regions, with their number and extent being dependent on the phase state of SS. Table 4 gives the number of invar regions of cell volume and the temperature interval of the widest regions in the cubic phase of SS of the PZT system.

2.5. The real phase diagram of SS of the PZT system

Based on the obtained results we have built the real diagram of states of the PZT system, which is shown in Fig. 15. It should be noted that on the whole the x-T diagram is similar to the one established earlier, but possesses a number of characteristic features, which were discussed above. In addition to the already described features, one should note the irregularity of the phase transition lines to the nonpolar phase, which is manifested to a greater extent in the region of Rh-T transition; the different extent of MR and differing characters of its changes: convergent ($R\rightarrow$Rh) and "funnelled" widening (Rh$\rightarrow T$) upon increasing T; the maximal concentration of regions of phase coexistence states in the Rh region at $x\geq 0.20$ and on "both sides" of MR (Rh$\rightarrow T$), which we relate to the defective nature of the studied ceramic SS.

3. Conclusions

As a result of high-temperature studies of SS of the PZT system the following fundamental differences from the traditional x-T phase diagram were revealed:

- at $x>0.20$ the transition to the C phase occurs not through the T phase, but through the "unclear symmetry region", which extends up to pure $PbTiO_3$ and is characterized by temperature-temporal instability;
- in the Rh phase at $x\leq 0.20$ the single-phase state remains until the transition to the C phase, whereas at $x>0.20$ upon increasing temperature successive changes of single-phase regions and regions of phase state coexistence occur, which can be the result of oxygen octahedral rotations;
- the T region is characterized by lesser (in comparison to Rh) saturation of the regions of phase state coexistence;
- the transition line to the nonpolar C phase is irregular, in particular at Rh$\rightarrow T$ transition;
- the extent of morphotropic regions is different and changes with increasing temperature in different ways: converges upon $R\rightarrow$Rh transition and "funnelled" widens at Rh$\rightarrow T$ transition.

The obtained results are expedient to use when interpreting the peculiarities of the formation of macroscopic properties of ceramics based on the PZT system.

Acknowledgments

We appreciate the help of Nikita Ter-Oganessian with the preparation of the manuscript. This work was financially supported by the Ministry of Education and Science of the Russian Federation, State contract no 16.513.11.3032.

References

[1] L.A. Reznichenko, L.A. Shilkina, O.N. Razumovskaya, E.A. Yaroslavtseva, et al., Phase x-T diagram of actual solid solutions of the $(1-x)PbZrO_3-{}_xPbTiO_3$ system ($0.37\leq x\leq 0.57$), Physics of the Solid State 50 (8) (2008) 1527–1533.
[2] I.N. Andryushina, L.A. Reznichenko, V.A. Alyoshin, L.A. Shilkina, et al., The PZT system ($PbZr_{1-x}Ti_xO_3$, $0.0\leq x\leq 1.0$): specific features of recrystallization sintering and microstructures of solid solutions (Part 1), Ceramics International (2012) 06.088.
[3] C.N.R. Rao, J. Gopalakrishnan, New Directions in Solid State Chemistry: Structure, Synthesis, Properties, Reactivity and Materials Design, Cambridge University Press, Cambridge, UK, 1986.
[4] L.A. Reznichenko, L.A. Shilkina, E.S. Gagarina, et al., Structural instabilities, incommensurate modulations and P and Q phases in sodium niobate in the temperature range 300–500 K, Crystallography Reports 48 (3) (2003) 448–456.
[5] V.V. Akhnazarova, L.A. Shilkina, O.Yu. Kravchenko, L.A. Reznichenko, Phase pattern of sodium niobate ceramics with different porosities in the temperature range of 25–700 °C, Crystallography Reports 56 (2) (2011) 282–288.
[6] L.A. Reznichenko, L.A. Shilkina, O.N. Razumovskaya, E.A. Yaroslavtseva, et al., Phase formation in near-morphotropic region of the $PbZr_{1-x}Ti_xO_3$ system, structural defects, and electromechanical properties of the solid solutions, Physics of the Solid State 51 (5) (2009) 1010–1018.
[7] I.N. Andryushina, L.A. Reznichenko, L.A. Shilkina, et al., The PZT system ($PbTi_xZr_{1-x}O_3$, $0\leq x\leq 1.0$): the real phase diagram of solid solutions (room temperature) (Part 2), Ceramics International (2012) 07.060.
[8] V.V. Eremkin, V.G. Smotrakov, E.G. Fesenko, Fazovie perehodi v sisteme tverdih rastvorov cirkonata-titanata svinca, Fizika Tverdogo Tela 31 (6) (1989) 156–162.
[9] A.J.C. Vilson, X-Ray Optics: The Diffraction of X-Ray by Finite and Imperfect Crystals, Methuen, 1962.
[10] L.S. Palatnik, A.A. Koz'ma, I.F. Mikhaĭlov, V.N. Maslov, Opredelenie harakteristik periodicheskih struktur po satellitam breggovskih otrazsheniy [Soviet Physics Crystallography], Kristallografiya 23 (1978) 570.
[11] B. Jaffe, W.R. Cook Jr., H. Jaffe, Piezoelectric Ceramics, Academic Press, London and New York, 1971.
[12] P. Bardhan, J.B. Cohen, Structural study of the alloy above its critical temperature, Acta Crystallographica A 32 (2) (1976) 597–614.
[13] A.A. Bondar, T.Ya. Velikanova, V.M. Danilenko, et al., Stabilnost faz III fazovie ravnovesia v splavah perehodnih metallov, Naukova Dumka, Kiev, 1991.
[14] A.I. Ustinov, L.A. Olikhovskaya, I.M. Shmytko, X-ray diffraction by polydomain crystals modulated by transverse waves of atomic displacements. 1. Single-wave modulation in crystals, Crystallography Reports 45 (3) (2000) 365–373.
[15] U.D. Tretiakov, Himiya nestehiometricheskih okislov, Izdatelstvo Moskovskogo gosudarstvennogo universiteta, Moscow, 1974.
[16] A.I. Ustinov, L.A. Olikhovskaya, I.M. Shmytko, X-ray diffraction in polydomain crystals modulated by transverse waves of atomic

displacements. 2. Two-wave modulation of crystals, Crystallography Reports 45 (3) (2000) 374–379.
[17] T. Miyanaga, D. Diop, S. Ikeda, H. Kon, Study of the local structure changes in $PbTiO_3$ by Pb L III EXAFS, Ferroelectrics 274 (2002) 41–53.
[18 K. Sato, T. Miyanaga, S. Ikeda, D. Diop, EXAFS study of the local structure change in perovskite titanates, Physica Scripta 115 (2005) 359–361.
[19] T. Miyanaga, K. Sato, S. Ikeda, D. Diop, Local structure changes in perovskite-type compounds by X-ray absorption find structure, Environmental Challenges (2002) 792–800.
[20] V.V. Eremkin, V.G. Smotrakov, E.G. Fesenko, Structural phase transitions in $PbZr_{1-x}Ti_xO_3$ crystals, Ferroelectrics 110 (1990) 137–144.
[21] A.M. Glazer, S.A. Mabud, Powder profile refinement of lead zirconate titanate at several temperature II pure $PbTiO_3$, Acta Crystallography 34 (1978) 1065–1070.
[22] G.A.Jr. Rossetti, A. Navrotsky, Calorimetric investigation of the tricritical behavior in tetragonal $Pb(Zr_xTi_{1-x})O_3$, Journal of Solid State Chemistry 144 (1999) 188–194.